Permeation properties of three-dimensional self-affine reconstructions of porous materials

E. S. Kikkinides* and V. N. Burganos†
Institute of Chemical Engineering and High Temperature Chemical Processes, Foundation for Research and Technology, Hellas, P.O. Box 1414, GR 265 00, Patras, Greece
(Received 9 March 2000)

A binary medium generation method is presented, which is capable of producing three-dimensional reconstructions of porous solids. The method is based on the midpoint displacement and successive random addition technique, which is, essentially, a graphical reproduction technique for the generation of self-affine media that follow fractional Brownian motion (FBM) statistics. Thresholding of the site values at the desired porosity value leads to three-dimensional porous constructions, the correlation degree of which is defined by the preselected value of the Hurst exponent. The correlation length of such single-cell media is comparable to the size of the working cell and, therefore, this approach would be of local use only. To remedy this problem, a method for producing multicell FBM media is presented, which is capable of generating media with size considerably larger than the correlation length and, as such, they can be employed to simulate a variety of actual porous solids. The percolation properties of these reconstructions are investigated and the specific surface area is calculated as a function of the porosity, the number of interwoven cells, and the Hurst exponent value. Furthermore, the flow equations are solved numerically within the void space of the three-dimensional FBM media and the effects of structure porosity and correlation degree on the permeability are studied. Application of the methodology to a sandstone sample as a case study showed a very good agreement of the numerical predictions for the permeability with actual permeability measurements and with the permeability estimate using a serial sectioning technique.

PACS number(s): 81.05.Rm, 47.55.Mh, 47.53.+n, 05.40.−a

I. INTRODUCTION

It has been recently realized that many natural porous media and aquifers exhibit long-range correlations [1], which are responsible for their unusual transport and percolation characteristics compared to those of disordered media with short-range correlations, or even of random media [2–3]. A special class of long-range correlations is the one that follows the statistics of fractional Brownian motion (FBM) [4]. This property appears to characterize a number of natural systems [5], and relates to the structural and transport properties of heterogeneous porous media (see, for example, [1–5] and the references cited therein).

In a recent publication [6], the authors presented a method for the reconstruction of porous media by generating two-dimensional lattices that follow FBM statistics. A modification of the conventional midpoint displacement and successive random addition method was employed in that work in order to generate multicell, interwoven binary media with sizes that are considerably larger than the correlation length of the medium. It was found that multicell FBM porous media possess very interesting structural properties that are functions of the Hurst exponent, a parameter characterizing the FBM stochastic process [4], and the porosity of the medium, only. In addition, they exhibit stronger structural correlation, lower specific surface area, higher percolation threshold, and lower permeabilities than those of the corresponding traditional single-cell FBM media. It was found that the construction of interwoven FBM binary lattices can lead to a robust representation of porous media, with improved behavior of their structural properties compared to that encountered in traditional, single-cell FBM lattices.

The applicability of the method to generate images that resemble real porous media was already demonstrated in [6]. Raw experimental data, namely, the porosity and autocorrelation function, can be used to adjust the reconstructed images to samples of the real solids under investigation. More specifically, microphotographing of thin sections of the material followed by image processing can yield information about the porosity and autocorrelation function, the statistical adequacy of which depends mainly on the homogeneity and isotropy of the material. Subsequently, FBM media can be generated that match these two structural properties, though in two dimensions, assuming invariance along the third one. The range of structural and flow properties of such porous reconstructions can be very broad, so that different classes of porous media can be efficiently simulated using this method. In addition, the method is relatively simple to use and offers an alternative to other stochastic reconstruction approaches (see, for instance, [7], and references therein), which can prove tedious for routine applications.

In the present paper, the limitation of the method to two dimensions is removed. We describe the generation of three-dimensional porous structures using a midpoint displacement method, suitably adjusted to apply to cubic lattices. The resulting media follow FBM statistics and, as in the conventional two-dimensional single-cell case, the correlation length is comparable to their overall size for finite correlation degree. In order to overcome this problem, we have modified the construction procedure so that multiple cells can be generated that share the same structural properties but are prop-

*Permanent address: Chemical Process Engineering Research Institute, P.O. Box 361, GR 570 01, Thermi, Thessaloniki, Greece.
†Corresponding author. Electronic address: vbur@iceht.forth.gr

erly interwoven so that continuity across their boundaries is ensured. The size of the three-dimensional structures that are generated in this manner is much larger than the correlation length and, consequently, average properties can be obtained that are independent of the size of the working sample. In addition, these multicell media are shown to follow FBM statistics and to share the same Hurst exponent value as that used for the construction of the basic cells. Percolation properties are determined for various working sample sizes and the effect of the interweaving process is discussed. The specific surface area is also calculated and a comparison between the single-cell and the multicell cases is made. The absolute permeability is subsequently calculated as a function of the correlation degree.

The methodology is applied to a Vosges sandstone sample, for which sufficient experimental data are available for the sake of comparison with the model results. Multicell FBM media are generated that match the porosity and the autocorrelation function determined experimentally through digitization of thin sections of the sample. It is found that the permeability estimate compares well with the measured value and the agreement improves as the number of cells used to generate the medium is increased. The specific surface area of the generated medium is also found to compare satisfactorily with the corresponding value obtained from serial tomography. Given that for engineering applications even an order-of-magnitude estimate of the permeability is considered a success, the convergence of our results to within a few percent from the available experimental value is very encouraging, especially since a minimal amount of information is needed for the reconstruction procedure. The agreement between our theoretical predictions and the experimental values justifies a further investigation of the applicability of the method to other reservoir rocks and other types of porous media that are known to exhibit long-range correlation [1–3].

II. GENERATION OF A BINARY MEDIUM FOLLOWING FBM STATISTICS

Following Mandelbrot and van Ness [4], one defines fractional Brownian motion $B_H(\boldsymbol{x})$ as a process that satisfies

$$\langle B_H(\boldsymbol{x}) - B_H(\boldsymbol{x}_0)\rangle = 0, \tag{1a}$$

$$\langle [B_H(\boldsymbol{x}) - B_H(\boldsymbol{x}_0)]^2\rangle \sim |\boldsymbol{x}-\boldsymbol{x}_0|^{2H}, \tag{1b}$$

where H is the Hurst exponent. For $H=\frac{1}{2}$, one recovers the classical Brownian motion. For $H>0$, FBM entails spatially growing correlations, whereas for strongly negative H values the medium becomes, practically, random. Excellent reviews regarding the properties of FBM can be found elsewhere [8–10].

Several variants of FBM have appeared in the literature. In a previous study [6], we described in detail how one can generate single-cell and multicell FBM lattices in two dimensions using the midpoint displacement method. In the present study, the method is extended to three dimensions and combined with successive random additions to yield three-dimensional self-affine media. Figure 1 (top) shows the first few stages involved in the construction of single-cell FBM lattices. Initially, one assigns random numbers from a

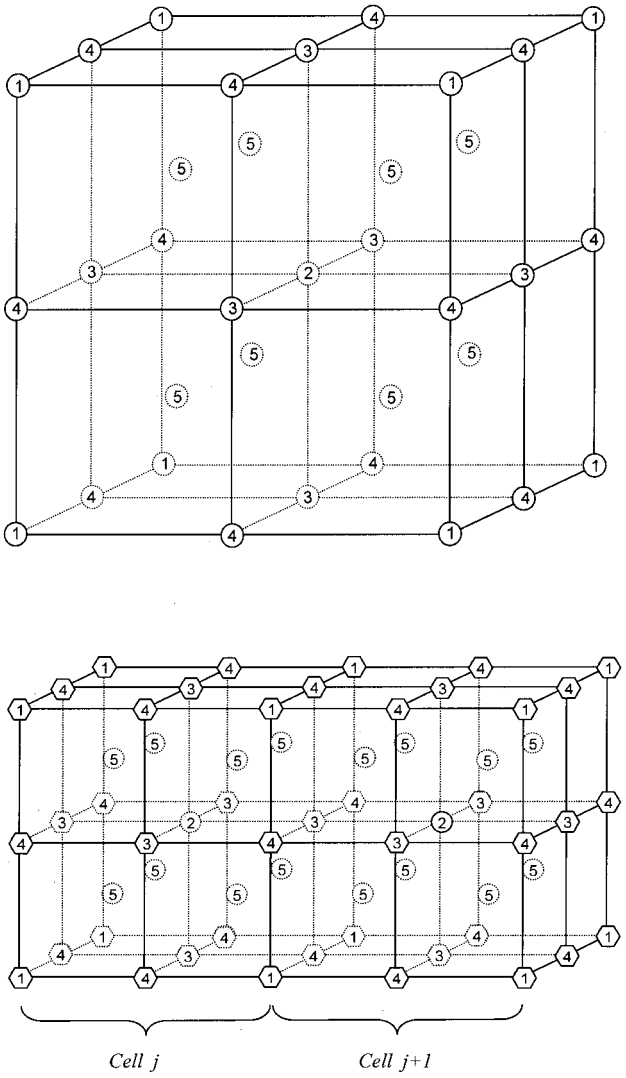

FIG. 1. Midpoint displacement in three dimensions. Top: startup cube in the single-cell case. Bottom: interweaving in the multicell case (averaging in polygon-shaped sites extends into adjacent cells).

Gaussian distribution with average 0 and standard deviation 1 at the eight corners of the starting three-dimensional (3D) cube (stage 1). Subsequently, the center of each cube is assigned the average of the values of the eight cube corners increased by an additional Gaussian deviate (stage 2). Next, the centers of the six faces of the cube are assigned values that are averages of the face corners, also increased by Gaussian deviates (stage 3). Then, the midpoints of the 12 edges of the cube are decorated as the averages of the corresponding endpoints increased by Gaussian deviates (stage 4). Thus, we have generated eight new smaller cubes inside the original cube and decorated the new sites using the midpoint displacement method. The above procedure, continued with the decoration of the centers of the eight new cubes (stage 5), is repeated several times until the desired resolution is achieved. The general rule is that at each new stage, the newly defined sites are assigned values that result from averaging the values of the closest neighboring sites and adding random deviates (midpoint displacement) with variance satisfying

$$\sigma_{n+1}^2 = r^{2H}\sigma_n^2. \tag{2}$$

In contrast to the two-dimensional case, the value of r that scales the resolution at each stage of the process is not constant, but changes with the type of site to be decorated. More specifically, $r=\sqrt{3}/2$ when decorating the body center, $r=1/\sqrt{2}$ when decorating the face centers, and $r=1/\sqrt{2}$ also when decorating the edge points in each cube, in this sequence.

The older sites can either retain their original values or be updated by a random addition of deviates with variance σ_{n+1}^2 (successive random addition). The above procedure generates a 3D lattice with sites following FBM statistics [2,5,6,8,9]. In order to transform it to a binary medium of a given porosity ε, one simply sorts the site values in a one-dimensional array of ascending order and assigns zero values to the lower part of the array with length $(1-\varepsilon)N_xN_yN_z$ and the value of one to the rest, where N_x, N_y, and N_z are the number of lattice points in the x, y and z direction, respectively. Note that throughout this study, unless otherwise indicated, it is assumed that $N_x=N_y=N_z=N$.

From a statistical point of view, such media cannot be used as valid representations of a real porous medium since they contain only a limited number of pores in each realization [6]. To remedy this, one can resort to interwoven multicell, 3D FBM lattices. This is accomplished in the present study following a procedure similar to the one introduced recently by the authors in the two-dimensional case [6]: The original lattice is divided into a number of smaller lattices, each of which is decorated according to the standard FBM procedure outlined above using a fixed value of H. However, the lattice points on the boundaries between adjacent sublattices receive contribution from all immediately neighboring cells during the averaging procedure. Figure 1 (bottom) shows two adjacent interwoven cells. Polygons are used to indicate boundary sites that are decorated using contributions from the immediate neighbors, whereas circles indicate internal sites that are assigned averages of sites that belong to the same cell. An illustration of the results of this construction technique for lattices with various numbers of individual cells N_p, while retaining the porosity and Hurst exponent values constant, is presented in Fig. 2. It is self-evident that the above modification can generate lattices with, practically, any degree of correlation desired, and sizes that are considerably larger than the correlation length.

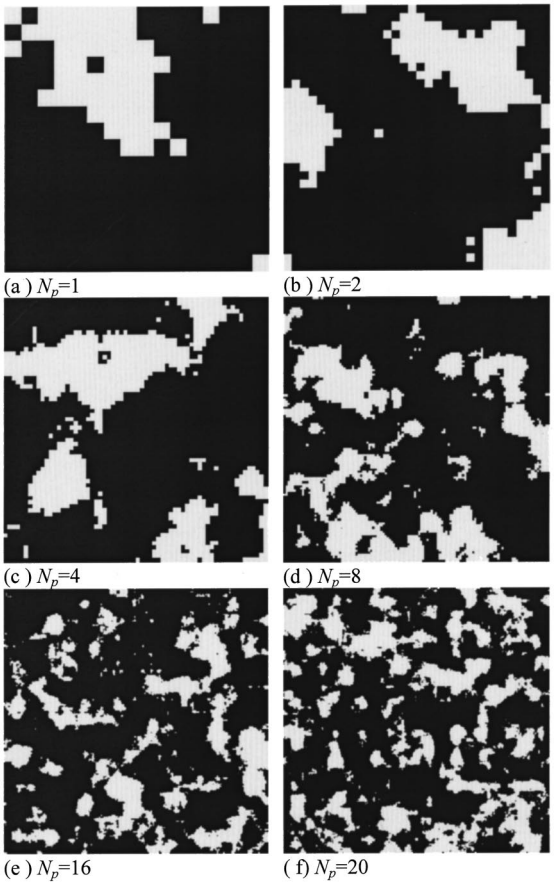

FIG. 2. 2D sections normal to the z axis of the 3D FBM lattice ($H=0.7$, $\varepsilon=0.2$, black: solid phase). Variation with the number of cells N_p, keeping the random number generator seed and the size of the unit cells constant ($N=8$).

III. STRUCTURAL PROPERTIES OF THREE-DIMENSIONAL FBM BINARY MEDIA

A. Correlation function

The correlation properties of reconstructed media are of critical importance for the assessment of their resemblance to actual materials. In terms of continuous variables, such as the local conductivity and permeability, percolation properties of FBM media have been determined in one and two dimensions by several authors using various definitions of correlation functions, semivariograms, etc. [1,10–12]. The main difference with the present line of work is that the FBM process is applied here to the structure itself and not to some transport property. Recently, the authors determined the two-point correlation function for 2D binary media that follow FBM statistics [6]. In the present work, the correlation function of 3D FBM media is calculated as the average of all 2D sections normal to a given direction, say the z axis.

Consider an actual 2D section of a porous medium. Using standard techniques [7,13], this section can be mapped on a 2D matrix of binary pixels, which take the values of 0 and 1 in the solid and pore phases, respectively. Accordingly, the phase function of the medium is defined as follows:

$$Z(\boldsymbol{x})=\begin{cases}1 & \text{if } \boldsymbol{x} \text{ belongs to the pore space}\\ 0 & \text{otherwise}\end{cases}, \tag{3}$$

where $\boldsymbol{x}$ is the position vector from an arbitrary origin. The porosity ε and the normalized two-point correlation function $R_z(\boldsymbol{u})$, can be defined by the statistical averages [7,13]

$$\varepsilon=\langle Z(\boldsymbol{x})\rangle \tag{4a}$$

$$R_z(\boldsymbol{u})=\frac{\langle[Z(\boldsymbol{x})-\varepsilon][Z(\boldsymbol{x}+\boldsymbol{u})-\varepsilon]\rangle}{\varepsilon-\varepsilon^2}. \tag{4b}$$

Note that $\langle\,\rangle$ indicates spatial average. For an isotropic medium, $R_z(\boldsymbol{u})$ becomes a function of $u=|\boldsymbol{u}|$ only [7]. A representative reconstruction of a medium in three dimensions should have the same correlation properties as those measured on a single two-dimensional section, expressed by the various moments of the phase function.

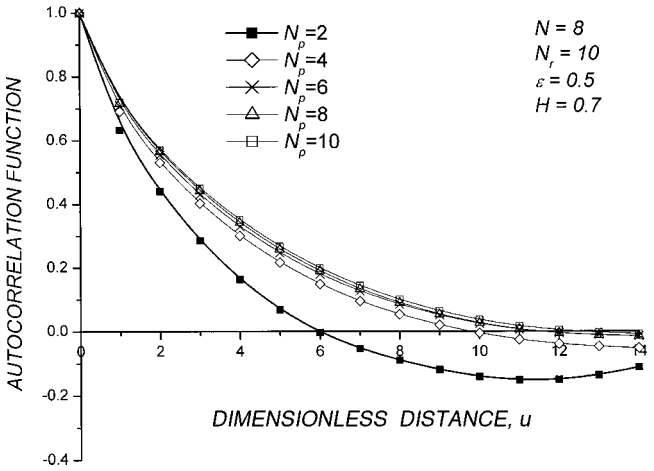

FIG. 3. Effect of the number of FBM cells (N_p) on the autocorrelation function, averaged over 10 realizations, keeping the size of each individual cell constant ($N=8$). $H=0.7$, $\varepsilon=0.5$.

It is interesting to examine the variation of the correlation function with the number of cells in the multicell FBM lattice, shown in Fig. 3 for $H=0.7$ and $\varepsilon=0.5$. The distance is expressed as the number of pixels, for easier scaling. The same definition is used for the distance throughout this paper, unless otherwise noted. Figure 3 reveals that the correlation curve is affected rather weakly by the number of cells, and for $N_p>6$, it remains practically unchanged. This is a quite useful property of multicell media, implying that the correlation properties are independent of the size of the working sample. It is also interesting to investigate possible anisotropy effects in the 3D multicell FBM media. To this end, the correlation functions in each principal direction were calculated by averaging all 2D sections along each direction. As shown in Fig. 4(a), all three curves for $N_p=8$ almost coincide, thus verifying isotropy in the structural properties of the multicell FBM 3D lattice.

It is interesting at this point to observe the effect of the Hurst exponent on the morphology of the FBM structures, following thresholding of the generated deviates at the porosity value. As illustrated in Fig. 5 ($\varepsilon=0.2$), high values of

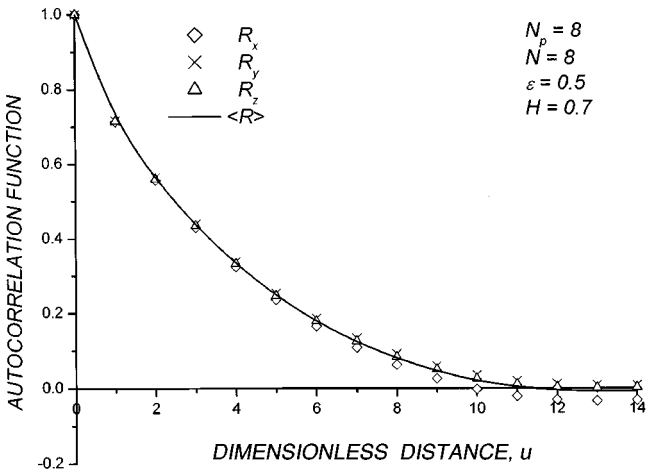

FIG. 4. Comparison of the average autocorrelation functions taken over all 2D sections cut across each principal direction of a 3D FBM lattice with $H=0.7$ and $\varepsilon=0.5$ ($N_p=N=8$).

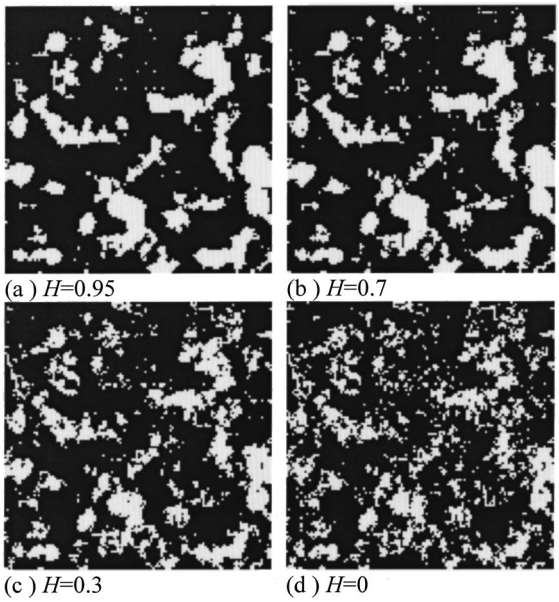

FIG. 5. 2D sections normal to the z axis of 3D FBM lattices ($\varepsilon=0.2$, black: solid phase). Variation with the value of the Hurst exponent H, keeping the random number generator seed constant ($N_p=16$, $N=8$).

H ($H>\frac{1}{2}$) lead to strongly correlated porous structures, whereas values of $H<\frac{1}{2}$ lead to less correlated structures. Sufficiently negative values of H yield, practically, uncorrelated media. A quantification of this observation is given in Fig. 6, where the corresponding correlation functions are plotted against distance, expressed as the number of pixels, for different values of H. As H decreases, the degree of correlation decreases too, in accord with the visual inspection of the corresponding images of Fig. 5. Furthermore, increasing the lattice size of each cell N, while keeping the rest of the parameters constant, results in stronger correlation. However, since the pixel size of the lattice is also decreased by the same factor, if the correlation function is plotted in terms of actual distance, that is, in length units and not in pixel-number units, the resulting curve coincides with the one ob-

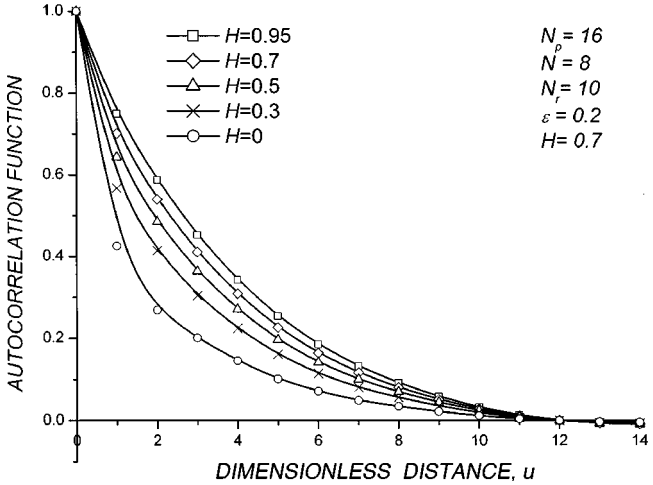

FIG. 6. Effect of the Hurst exponent value on the autocorrelation function of multicell FBM media ($N_r=10$, $\varepsilon=0.2$, $N_p=16$, $N=8$).

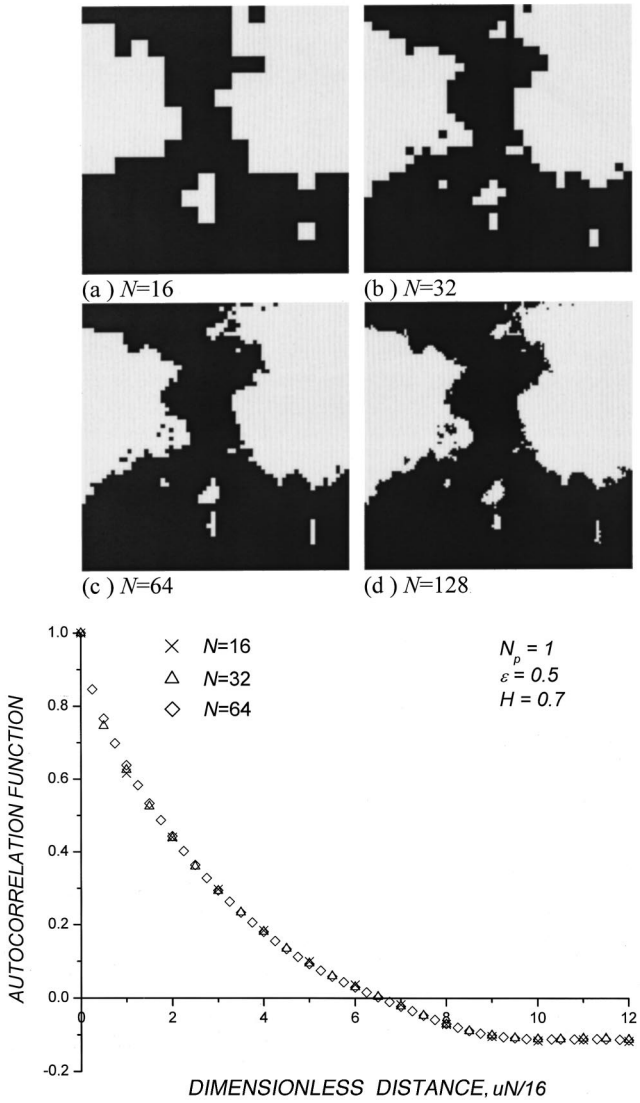

FIG. 7. Effect of the lattice size on the construction of single-cell 3D FBM media, using the same random number generator seed ($\varepsilon=0.5$, $H=0.7$, $N_p=1$). (a) Morphology of generated images. (b) Correlation function of generated media. The distance is rendered dimensionless using as reference the pixel size in the $N=16$ case.

tained for the original lattice. This was also the case for 2D FBM media [6]. This result is illustrated in Fig. 7, in the form of image morphology (a) and corresponding correlation function (b). Note that the abscissa in Fig. 7(b) is the distance between two points, rendered dimensionless using the pixel size in a given lattice size ($N=16$) as reference ($uN/16$). This choice was made to avoid automatic scaling with the change of the lattice size. It is confirmed that the curve of the correlation function remains, practically unchanged when the lattice size of the FBM medium is altered.

B. Surface area

The evaluation of the internal surface area of a porous medium is of primary significance in the modeling of fluid-solid interaction phenomena, such as sorption, surface diffusion, chemical reaction, infiltration, etc. In the context of the present paper, it is very interesting to investigate the effects

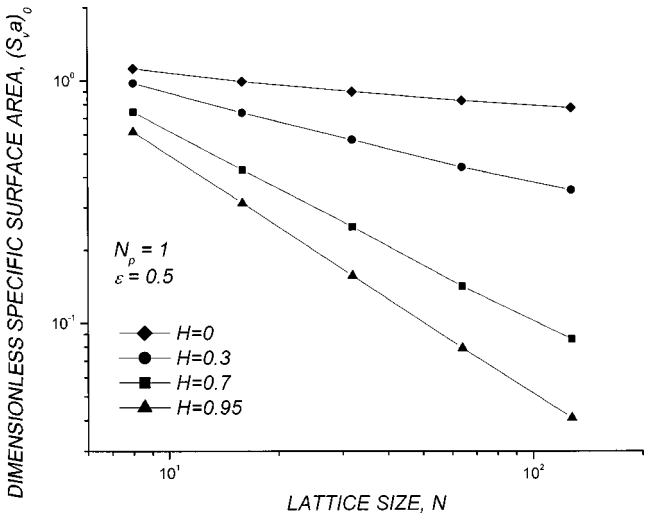

FIG. 8. Dimensionless specific surface area vs lattice size, for single-cell FBM media.

of the construction algorithm and parameters on the specific surface area of the generated media, and ensure that the construction procedure provides the necessary flexibility to cover a broad range of specific surface area values, so that it can be applied to simulate actual porous materials.

In the limiting case of completely randomized binary media, the specific surface area is given by

$$S_{v,\mathrm{random}}=\frac{6\varepsilon(1-\varepsilon)}{a}, \tag{5}$$

where a is the size of the unit element, following a rigorous proof by Burganos [14]. For correlated media, it is known that the specific surface area can also be determined from the slope of the autocorrelation function, $R_z(u)$, evaluated at $u=0$ [15]:

$$S_v=-6(\varepsilon-\varepsilon^2)R_z'(0). \tag{6}$$

The calculation of the internal surface area of discretized media can be implemented through identification and counting of the solid/void interface segments, based on the identification code (0/1). The results for single-cell FBM media are shown in Fig. 8, plotted against the lattice size, N. For sufficiently large lattices, linearity is obtained in log-log scale for all Hurst exponent values in the interval [0,1] examined here. That is,

$$\frac{S_{v1}}{S_{v2}}=\left(\frac{a_1}{a_2}\right)^{\beta-1}, \tag{7}$$

where β is the negative of the slope of the lines and is characteristic of the correlation degree of the medium. In fact, it practically coincides with the Hurst exponent value H, which verifies that the generated media follow FBM statistics: $d_F=3-H$ is the fractal dimension of a zeroset of an FBM process in three dimensions and $S_v \propto a^{2-d_F}$, that is, $S_v a \propto N^{-H}$.

Switching from single-cell to multicell media results in increased correlation, as shown in Fig. 3. This implies that as the number of patches N_p, increases, the specific surface

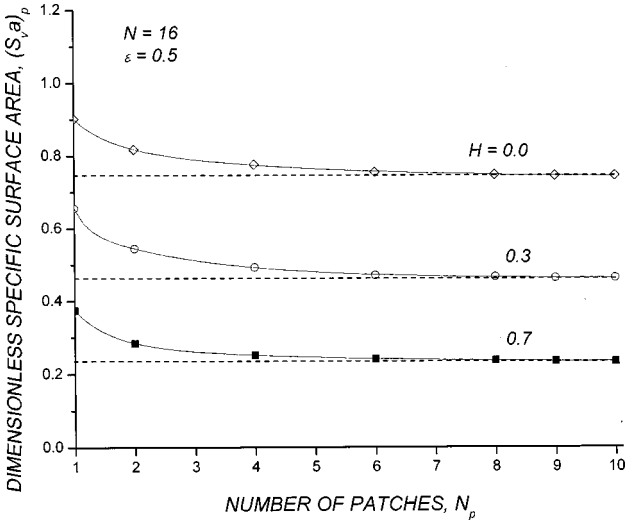

FIG. 9. Dependence of the dimensionless specific surface area on the number of patches in 3D, multicell FBM media. Variation with the Hurst exponent value *H*.

area should decrease. This is indeed the case, as seen in Fig. 9. It is also noteworthy that the specific surface area attains a limiting value for sufficiently large N_p values, which is characteristic of the porosity and the Hurst exponent value. This constitutes an advantage of multicell media compared to single-cell reconstructions, which suffer from the dependence of the dimensionless specific surface area on the overall size of the medium. The surface area of multicell media decreases upon increasing the value of *H* (or, equivalently, upon intensifying the structure correlation), as confirmed in Fig. 9.

An additional property of the multicell media that are constructed in the aforementioned manner is that they do follow FBM statistics, just as their unit cells. Figure 10 shows the dependence of the specific surface area of three-dimensional multicell media on the lattice size of the basic cells for various values of the Hurst exponent. Note the linearity of the corresponding curves for low, intermediate, and

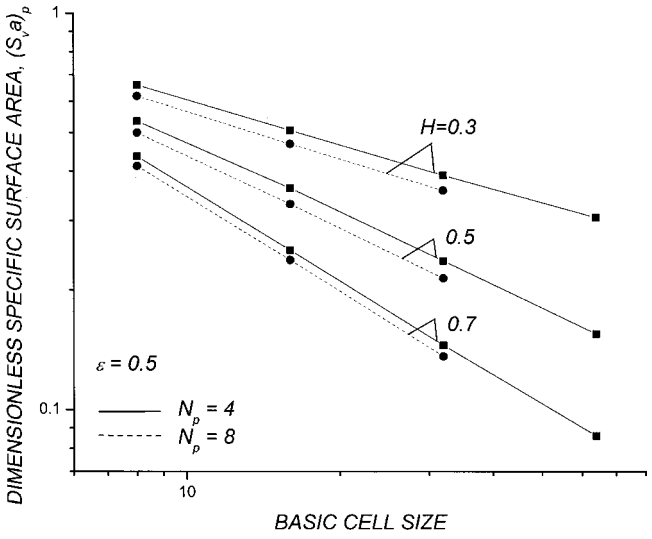

FIG. 10. Dimensionless specific surface area vs lattice size of the basic cell, for multicell 3D media.

high *H* values, which implies the validity of Eq. (7) also for multicell media. The slope of the lines is approximately equal to the negative of the Hurst exponent, just as in the single-cell case. The only difference is that the computational requirements for the multicell media are heavier than in the single-cell case by a factor of N_p^3 and, consequently, detailed calculations at the limit of large unit cell sizes (N) are prohibited by, mainly, computer memory limitations. Nevertheless, Fig. 9 indicates that the value $N_p=8$ is sufficiently high for convergence with respect to the number of cells and, consequently, it may be argued that the linearity of the curves in Fig. 10 is of general validity for multicell media and with fractal dimension that satisfies $d_F=3-H$, just as in the single-cell case. Thus, it is claimed that the three-dimensional media generated here are indeed self-affine, FBM structures.

C. Percolation properties

Early and recent studies have shown that binary media with long-range correlations show completely different percolation properties, in terms of percolation threshold and/or scaling characteristics, from those of random or even short-range systems [10,16–18]. A notable conclusion of detailed percolation studies on 2D systems that follow FBM statistics [2,6,18] is that the percolation threshold, p_c, of these media is a random variable with a mean value $\langle p_c \rangle$, that decreases with increasing *H* in a monotonic fashion. Moreover, the construction of multicell 2D FBM lattices [6] leads to decreased statistical deviations of their percolation properties but also favors clustering of large cavities, thus giving rise to increased percolation threshold values.

In the present study, mean percolation threshold and standard deviation values are determined for single-cell and multicell 3D lattices constructed by the midpoint displacement technique. Following the studies of the corresponding 2D media, in the present work we investigate the effects of the number of cells (or number of patches, N_p), and the value of the Hurst exponent *H*, on the percolation threshold properties of 3D FBM media, using a large number of realizations for each data set. The cluster labeling algorithm proposed by Hoshen and Copelman [19], and described also by Stauffer and Aharony [20], is employed in the present study to determine the percolation threshold.

The numerical results of this investigation are summarized in Table I. The values for the average percolation threshold in 3D FBM lattices are considerably lower compared to the corresponding 2D cases, as expected. Moreover, keeping the lattice size constant ($N=16$), the average percolation threshold decreases as the number of cells increases, until a constant value is attained for a sufficiently large number of cells ($N_p>8$). Hence, in the case of 3D FBM lattices, the interweaving process tends to connect isolated clusters that exist in the single cells, resulting in the formation of alternate paths to percolation and, consequently, in a lower percolation threshold compared to the single-cell case. The standard deviation, on the other hand, decreases considerably as the number of cells increases, confirming the statistical validity of multicell FBM lattices in terms of their structural properties.

Finally, the effect of the degree of correlation, expressed in terms of the Hurst exponent value *H*, on the average per-

TABLE I. Percolation threshold values for single and multicell FBM lattices. Number of realizations: 500. *Note*: Values reported here correspond to percolation through either principal direction.

	Single-cell	Multicell reconstructions			
H	$N_p=1$, $N=64$	$N_p=2$, $N=16$	$N_p=4$, $N=16$	$N_p=8$, $N=16$	$N_p=10$, $N=16$
0.95	0.083 ± 0.062	0.104 ± 0.051	0.097 ± 0.033	0.087 ± 0.021	0.087 ± 0.016
0.7	0.084 ± 0.053	0.104 ± 0.048	0.096 ± 0.031	0.088 ± 0.020	0.087 ± 0.016
0.3	0.083 ± 0.037	0.108 ± 0.040	0.096 ± 0.027	0.090 ± 0.017	0.089 ± 0.015
0.0	0.109 ± 0.028	0.130 ± 0.035	0.111 ± 0.025	0.105 ± 0.016	0.106 ± 0.013

colation threshold values appears relatively weak compared to the 2D case, especially for $H>0.3$, probably due to the increased connectivity obtained upon switching from two to three dimensions, which facilitates permeation drastically and reduces the percolation threshold to relatively low values. It is also noteworthy that the standard deviation of the $\langle p_c \rangle$ estimates decreases as H decreases, as was also the case with the corresponding calculations in 2D FBM media [6].

IV. FLOW IN A THREE-DIMENSIONAL FBM POROUS MEDIUM

A. Calculation of the flow field

The creeping flow of a Newtonian fluid in the interstitial space of a porous medium is described by the Stokes equation coupled with the continuity equation:

$$\nabla P = \mu \nabla^2 \boldsymbol{v}, \tag{8a}$$

$$\boldsymbol{\nabla} \cdot \boldsymbol{v} = 0, \tag{8b}$$

where $\boldsymbol{v}$ and P are the local velocity and pressure of the fluid, respectively. The boundary conditions for $\boldsymbol{v}$ are spatial periodicity and no-slip at the surface of the solid unit elements. A macroscopic pressure gradient ∇P is specified and the seepage velocity $\langle \boldsymbol{v} \rangle$, defined as the superficial velocity averaged over a cross section of the medium, is related to ∇P by the permeability tensor $\boldsymbol{K}$, as follows:

$$\langle \boldsymbol{v} \rangle = -(\boldsymbol{K}/\mu) \cdot \boldsymbol{\nabla} P. \tag{9}$$

$\boldsymbol{K}$ is a symmetric tensor that depends only on the geometry of the system. For isotropic media,

$$\boldsymbol{K} = K\boldsymbol{I}, \tag{10}$$

where $\boldsymbol{I}$ is the unit tensor.

Hence, in order to determine the permeability from Eq. (9), one needs to calculate first the flow field by solving the flow and continuity Eq. (8) with the appropriate boundary conditions. The numerical method employed in this work is similar to the one used by Adler and coworkers [7,21]. A finite difference scheme using the marker and cell (MAC) method [22] was employed. More specifically, a staggered marker-and-cell mesh is used, with the pressure defined at the center of the cell, and the velocity components defined along the corresponding face boundaries of the cell. Successive overrelaxation (SOR) and conjugate gradient (CG) methods were used to solve for the microscopic velocity field. In order to cope with the numerical instabilities caused by the continuity equation, an artificial compressibility technique was employed [6,22], according to which an accumulation term for the pressure is included in Eq. (8b). In this fashion, the steady-state problem is replaced by an unsteady one, which converges to the incompressible steady-state solution for a sufficiently long time.

The mesh spacing in each direction is a fraction of the size of the unit elements. More specifically, it is expressed here as $\Delta x = \Delta y = \Delta z = a_N / N_s$, where N_s is an integer denoting the discretization level inside each void unit element of size a_N. Convergence was achieved when the calculated flow rate values were found to fluctuate less than 1% across the various cross sections of the medium. For a given realization, it was found that N_s can have some nonnegligible impact on the permeability value K, in full agreement with earlier studies [21]. Nevertheless, the effect of N_s tends to diminish as the value of N increases, or, equivalently, as the size of the unit element a decreases sufficiently. In general, convergence was relatively rapid in the medium and high porosity region ($\varepsilon>0.4$), whereas it was significantly slower in the vicinity of the percolation threshold ($\varepsilon<0.2$). This is attributed to the fact that, in the latter case, large isolated regions are likely to develop, which may be connected via narrow necks, that apparently hinder the updating of the velocity and pressure values across the porous medium.

B. Permeability results

The average permeability of porous media generated by FBM lattices has been determined for different structural parameters, such as lattice size N, number of cells N_p, porosity ε, and degree of correlation, obtained by varying the value of the Hurst exponent H. The results are averaged over a number of random realizations, constructed with the same set of structural parameters, in order to limit possible statistical errors. Given the relatively large size of the 3D working samples ($N_p N = 64$) used in most of our computations, a relatively small number of realizations (10) was found to suffice for statistically meaningful permeability results [21].

Figure 11 presents the effect of the lattice size N on the value of permeability, for a single-cell FBM medium, at high (0.8) and moderate (0.4) porosity values. Doubling the lattice size N yields a fourfold increase of the value of K/a^2, for sufficiently large cells ($N \geqslant 16$). Since doubling the value of N translates to reduction of the unit element side by the factor of 2, the aforementioned fourfold increase of the dimensionless permeability implies that the dimensional value of the permeability, K, remains constant. In other words, for sufficiently large lattices ($N \geqslant 16$), the absolute permeability

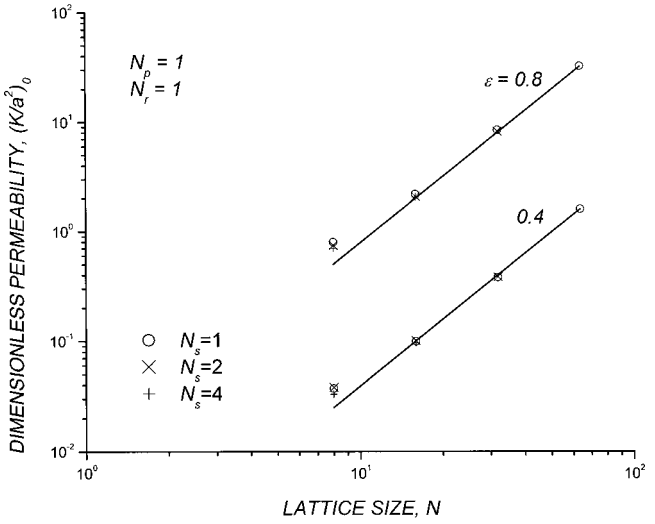

FIG. 11. Dimensionless permeability vs lattice size for single-cell FBM media ($N_p=1$, $N_r=1$). Effect of the discretization parameter N_s.

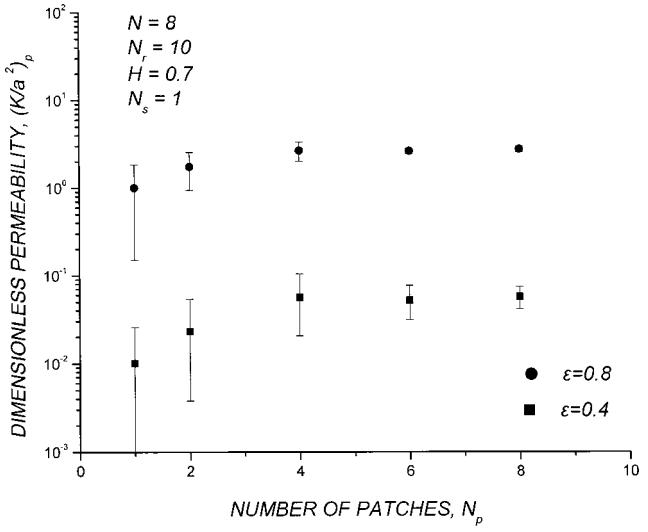

FIG. 13. Variation of the dimensionless permeability of 3D FBM media with the number of cells N_p for high and intermediate porosity values ($N=8$, $H=0.7$, $N_r=10$, $N_s=1$).

is invariant with respect to the resolution of the lattice. Note that in the same figure, permeability estimates for different values of the discretization parameter N_s are indicated. As expected, the smaller the lattice size the stronger the effect of N_s on the numerical estimate of the permeability. More specifically, in the case of high porosity media ($\varepsilon=0.8$) with $N=8$, the relative change in permeability is around 13.7% when switching from $N_s=1$ to $N_s=4$, whereas for $N=16$ this change drops to about 6%. The corresponding values in the case of $\varepsilon=0.4$ are 12.6% and 3.3%, respectively. Therefore, when studying the resolution effect on the flow properties of FBM generated structures, one should take into consideration the lattice size, N, in conjunction with the discretization parameter, N_s.

Figure 12 presents the dependence of the average permeability K, for $N_p=1$, $N=32$, and $N_s=1$, on the value of H for high (0.8) and moderate (0.4) porosity levels. As expected, the permeability increases with the value of the Hurst exponent H, for both porosity values examined here. It is interesting to note that the permeability of strongly correlated FBM media can become almost two orders of magnitude higher than that of weakly correlated porous media, even for moderate and high porosity values, that is, even away from the percolation threshold. This observation is in full alignment with the corresponding results for 2D FBM media [6], and implies that FBM porous media can be employed in the study of flow in actual porous media over a wide range of permeability values.

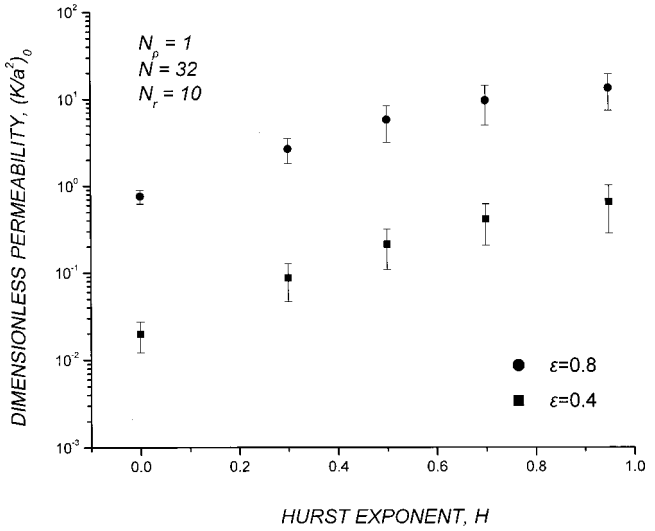

FIG. 12. Dependence of the dimensionless permeability of single-cell 3D FBM media on the value of the Hurst exponent ($N_p=1$, $N=32$, $N_r=10$).

Figure 12 reveals that relatively large error bars are obtained during permeability calculations for single-cell FBM media ($N_p=1$). If these calculations are repeated for a much larger number of cells (but with $N=8$ and $N_s=1$ to keep computational requirements within reason), significantly lower standard deviations for the same structural properties of the lattices are obtained. The permeability predictions for two porosity values varying the number of cells, N_p, are presented in Fig. 13. Note that for $N_p \geqslant 4$ the average permeability remains nearly constant, but the corresponding standard deviation keeps decreasing as the number of cells increases. Based on these results, it can be claimed that a value of $N_p=6$ is close to optimal, as it combines computational efficiency with statistical accuracy in terms of average and standard deviation values for the permeability. In addition, according to the results shown in Fig. 3, the autocorrelation function remains practically constant for $N_p \geqslant 6$.

V. APPLICATION

It was shown in a previous work [6] that 2D multicell lattices built with an FBM process could be potentially employed to simulate the structure of actual porous media. In particular, we showed there that images of Vosges sandstone samples could be effectively reproduced by employing the cell interweaving technique. In the present study, we reproduced three-dimensional images of Vosges sandstone and calculated the permeability of the reconstructions. The fol-

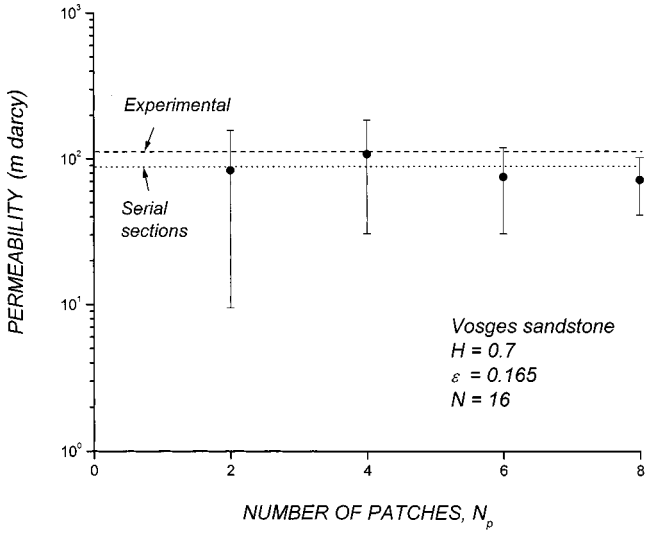

FIG. 14. Effect of the number of cells on the estimation of the permeability of Vosges sandstone using FBM media ($N=16$). Comparison with the experimental value and with the prediction of the serial sectioning technique.

lowing steps were taken: First, a reasonable lattice size was selected, which would allow not only reconstruction in three dimensions but also the numerical solution of the flow equations, with sufficient accuracy. A combination of pixel size and Hurst exponent values was found that allowed a satisfactory fit of the simulated correlation function curve with the experimental one [23]. The thresholding stage was straightforward and the desired porosity value was easily achieved ($\varepsilon=0.165$). Care was taken during the correlation function matching to express the distance in actual length units. Once the reconstruction was completed, the flow problem was solved, following the procedure described above. The average permeability was then calculated, using a sufficiently large number of realizations for statistically meaningful results to be obtained. In order to study the sensitivity of the methodology to the overall working sample size, the entire procedure was repeated for different values of N_p.

The results are presented in Fig. 14 and compared to the experimental value found in Ref. [23] and to the numerical estimate of the permeability based on serial tomography. More specifically, in a previous work [23], serial tomography was applied to this particular sample, which provided a series of 45 sequential sections, taken every 2.04 μm. The sections were digitized and the phase function was determined in three dimensions. The flow equations were then solved, again, using this time the actual digitized structure, with a resolution of 482×500 pixels in each section. The agreement between the FBM and the serial sectioning approaches is quite satisfactory, despite the rather small working samples employed in the FBM reconstructions due to computational constraints. In addition, the agreement with the experimental value is also satisfactory, taking into account the fact that the size of the sample studied was rather small (volume of sample 0.33 mm^3) compared to the scale of possible heterogeneities and the size of the sample used for the permeability measurement (order of cm). As expected, the effect of N_p is rather weak, provided $N_p\geqslant6$, in accord with the relevant discussion of Fig. 13, which means that the results of the methodology suggested here are, practically, insensitive to the overall size of the reconstruction.

In addition to the permeability investigation, we found it very tempting to compare the specific surface area of the reconstructed media to the actual specific surface area of the sample studied. The FBM reconstructions had, on the average, specific surface area equal to $0.55\times10^5\,m^{-1}$, which compares well with the value obtained from the serial tomography method, $0.52\times10^5\,m^{-1}$. The agreement is very good and is due to the matching of the corresponding autocorrelation functions, which, in turn, relate to the specific surface area through Eq. (6). The corresponding mean chord lengths are found to equal 12.0 and 12.7 μm respectively, using the well-known expression $d=4\varepsilon/S_v$. As expected, the agreement is again quite satisfactory.

VI. CONCLUSIONS AND FURTHER REMARKS

A methodology for the generation of three-dimensional images of porous media is presented, using a minimal set of raw experimental data, namely, microphotographs of two-dimensional sections. The methodology is based on the midpoint displacement and successive random addition technique, suitably adjusted to a cubic lattice. The resulting binary media follow classical FBM statistics to a good approximation, and appropriate thresholding at the desired porosity value can yield three-dimensional porous media in digitized form. The degree of structure correlation is adjusted through the Hurst exponent value, which, in turn, is selected in a fashion that allows sufficient matching of the autocorrelation function of the reconstruction with that measured on physical sections of the material. Thus, not only does the methodology presented here offer the flexibility to match experimental data for the porosity and the autocorrelation function, but it does so through a well-defined specific correlation process.

Evidently, the size of the resulting reconstructions is of the same order of magnitude as the correlation length, owing to the construction process, which is centered around the geometrical center of the working sample and yields long-range correlations. To overcome this problem, which is typical in these types of reconstructions, we have devised an algorithm that allows the generation of three-dimensional media made up of individual cells, each of which follow FBM statistics with the same value of the Hurst exponent. These cells are properly interwoven across their boundaries, so that a much larger medium is obtained, with a size considerably larger than the correlation length of the construction process. In this way, reconstructions that closely resemble actual porous media can be obtained, involving a significant number of individual ''pores.''

Numerical calculations showed that the Hurst exponent value can affect quite strongly the correlation degree of both single-cell and multicell FBM media. Increasing the H value results in stronger correlation for the same porosity value. In addition, as the number of individual cells, or patches, increases, the correlation degree also increases and the percolation threshold decreases to very low values. This is a particularly useful result toward the simulation of actual materials, in contrast to the use of random reconstructions, which exhibit rather high percolation thresholds. The specific

surface area of 3D single-cell FBM media is a function of the lattice size, and the calculated fractal dimension almost coincides with the fractal dimension of the zerosets of FBM processes in 3D, namely, $d_f=3-H$. As the H value increases, the specific surface area decreases, owing to the intensified clustering of void elements and the concomitant vanishing of solid walls. The specific surface area decreases with the increasing number of interwoven cells, until a limiting value is reached, beyond which the surface area remains unchanged. This is a very useful property of multicell FBM media, since the desired value of the specific surface area can be reached with no dependence on the overall size of the generated medium.

The Stokes equation for creeping flow conditions coupled with the continuity equation were solved numerically using SOR and CG techniques. The permeability of the reconstructed media was then calculated as a function of the porosity and the Hurst exponent value. Because of the reduction of the percolation threshold at relatively large H values, the calculation of finite permeabilities in low porosity media was made possible. The application to real porous solids was straightforward. Physical sections of the material were digitized and the porosity and autocorrelation function were determined with an appropriate image software. Subsequently, three-dimensional reconstructions were realized using the midpoint displacement and successive random addition technique described in this paper followed by thresholding at the desired porosity value. The value of the Hurst exponent was selected so that the simulated correlation function matched the experimental one. It was found that the calculated permeability values compared well with the measured values. The error was relatively small and could be due to a variety of reasons, including possible heterogeneity of the real solids, which would confine the validity of the calculated permeability value to the neighborhood of the thin section.

It must be stressed that the methodology developed in this paper uses a minimal amount of structural information to reconstruct the medium, namely, the porosity and autocorrelation function only. Theoretically, higher moments of the correlation function are needed for reliable reproduction of the pore structure. It is understood that the role of these moments cannot be rigorously substituted with simplified correlation algorithms, such as the FBM process. However, the methodology presented in this paper provides a simple means for the reconstruction of porous media, combining computational cost effectiveness, lumping correlation properties into few working parameters, and sufficient resilience toward matching of the generated media to actual porous materials.

ACKNOWLEDGMENTS

This work was supported financially by GSRT Grant No. PENED 99-485 and by the Institute of Chemical Engineering and High Temperature Chemical Processes–Foundation for Research and Technology, Hellas (ICE/HT-FORTH).

[1] T. A. Hewett, SPE Paper No. 15386 (unpublished).
[2] C. Du, C. Satic, and Y. C. Yortsos, AIChE J. **42**, 2392 (1996).
[3] M. Sahimi, AIChE J. **41**, 229 (1995).
[4] B. B. Mandelbrot and J. W. Van Ness, SIAM Rev. **10**, 422 (1968).
[5] R. F. Voss, in Fundamental Algorithms for Computer Graphics, Vol. 17 of *NATO Advanced Studies Institute, Series Computer and Systems Sciences*, edited by R. A. Ernshaw (Springer-Verlag, Berlin, 1985), p. 805.
[6] E. S. Kikkinides and V. N. Burganos, Phys. Rev. E **59**, 7185 (1999).
[7] P. M. Adler, C. J. Jacquin, and J. A. Quiblier, Int. J. Multiphase Flow **16**, 691 (1990); M. A. Ioannidis, M. J. Kwiecien, and I. Chatzis, J. Pet. Sci. Eng. **16**, 251 (1996).
[8] R. F. Voss, in *The Science of Fractal Images*, edited by H. O. Peitgen and D. Saupe (Springer-Verlag, Berlin, 1988).
[9] J. Feder, *Fractals* (Plenum, New York, 1988).
[10] M. B. Isichenko, Rev. Mod. Phys. **64**, 961 (1992).
[11] M. Sahimi, J. Phys. I **4**, 1263 (1994).
[12] S. Prakash, S. Havlin, M. Schwartz, and H. E. Stanley, Phys. Rev. A **46**, R1724 (1992).
[13] J. G. Berryman, J. Appl. Phys. **57**, 2374 (1985).
[14] V. N. Burganos, J. Chem. Phys. **109**, 6772 (1998).
[15] C. L. Y. Yeong and S. Torquato, Phys. Rev. E **57**, 495 (1998).
[16] A. B. Haris, J. Phys. C **7**, 1671 (1974).
[17] A. Weinrib and B. I. Halperin, Phys. Rev. B **27**, 413 (1983).
[18] S. Prakash, S. Havlin, M. Schwartz, and H. E. Stanley, Phys. Rev. A **46**, R1724 (1992); J. Schmittbuhl, J. P. Vilotte, and S. Roux, J. Phys. A **26**, 6115 (1994).
[19] J. Hoshen and R. Kopelman, Phys. Rev. B **14**, 3438 (1976).
[20] D. Stauffer and Aharony *Introduction to Percolation Theory* (Taylor Francis, London, 1992).
[21] R. Lemaitre and P. M. Adler, Transp. Porous Media **5**, 325 (1990).
[22] P. J. Roache *Computational Fluid Dynamics* (Hermosa, Albuquerque, NM, 1982).
[23] J. Yao, J. F. Thovert, P. M. Adler, C. D. Tsakiroglou, V. N. Burganos, A. C. Payatakes, J. C. Moulu, and F. Kalaydjian, Rev. Inst. Fr. Pet. **52**, 3 (1997).